In vitro modelling of anterior primitive streak patterning with hESC reveals the dynamic of WNT and NODAL signalling required to specify notochord progenitors

M. Robles Garcia[†], C. Thimonier[†], K. Angoura[†], E. Ozga[†], H. MacPherson, G. Blin[*]

Institute for Regeneration and Repair, Institute for Stem Cell Research, School of Biological Sciences, The University of Edinburgh, 5 Little France Drive, Edinburgh BioQuarter, Edinburgh EH16 4UU, UK.

† These authors contributed equally to this work.

* Author for correspondence (guillaume.blin@ed.ac.uk)

Abstract

Notochord progenitors (NotoPs) are a rare, yet vital embryonic cell population that give rise to the cells that form and maintain intervertebral discs. An unlimited access to NotoPs would open new opportunities for basic biomedical research and regenerative medicine of the discs. **However, the mechanisms responsible for the specification and the maintenance of NotoPs are not understood.** This gap in understanding stems from the fact that NotoPs emerge during the gastrulation to axial elongation transition; an event that is ethically and technically challenging to investigate.

Here, to circumvent this issue, we use micropatterning to guide the development of human ESCs into standardised patterns of anterior primitive streak cell fates. We found that endogenous levels of NODAL signalling regulate the balance of axial progenitors and that NotoPs emergence requires the timely inhibition of Nodal signalling.

Our work provides insights into the mechanisms driving the patterning of the of the axial progenitor niche and may inform the development of future strategies aimed at deriving bona-fide NotoPs from hESC.

Introduction

In vertebrate embryos, the tissues of the posterior axis, including the spinal cord, the cartilage, bones and muscles of the spine, as well as the gut, are all laid down progressively in an anterior-to-posterior direction. This evolutionary-conserved process, termed axial elongation (reviewed in (Henrique et al., 2015; Neijts et al., 2014; Wymeersch et al., 2021), is governed by lineage-restricted progenitors emerging during gastrulation in the anterior portion of the primitive streak (APS) (Fig1A).

Among these, notochord progenitors (NotoPs) give rise to the notochord, a cylindrical structure that forms along the ventral midline in chordate embryos (Balmer et al., 2016; Stemple, 2005). The notochord ensures essential functions during development, both as a source of localised signalling molecules necessary for the proper patterning of adjacent tissues (Streit and Stern, 1999) and as a mechanical structure contributing to the straightness of the rostro-caudal axis as the embryo elongates (Bagnat and Gray, 2020). Eventually, the cells that form the notochord contribute to the nucleus pulposus (Choi et al., 2008; McCann et al., 2012), the central region of intervertebral discs responsible for the homeostasis of the surrounding fibro-cartilagenous tissue (reviewed in (Wise et al., 2020)).

Previous work has shown that the specification of the notochord requires the cooperation of WNT and NODAL signalling (Dunn et al., 2004; Lickert et al., 2002; Merrill et al., 2004; Vincent et al., 2003; Yamamoto et al., 2001). However, the exact signalling requirements for the specification of NotoPs has remained elusive. Indeed, in spite of previous efforts (Colombier et al., 2020; Diaz-Hernandez et al., 2020; Winzi et al., 2011; Zhang et al., 2020), the derivation of NotoPs from pluripotent stem cells remains inefficient and leads to mixed population of cells including alternative cell fates from the mesoderm and endoderm lineage. Furthermore, apart from one exception (Xu et al., 2021), 3D organoids that mimic axial elongation also lack notochord in spite of the fact that WNT and NODAL signalling are both active in these in vitro models (Beccari et al., 2018; Cermola et al., 2021; Moris et al., 2020; Turner et al., 2017) suggesting there may be additional unknown cues needed for notochord specification.

This gap in understanding stems from the relative rarity of NotoPs in the embryo and from the complexity and rapidity of the cell fate decisions occurring in the APS. NotoPs emerge in close proximity to both the definitive endoderm (Beddington and Robertson, 1989; Scheibner et al., 2021), and neuromesodermal progenitors (NMPs), the bi-fated cells that form the somitic mesoderm and the spinal cord (Cambray and Wilson, 2002; Cambray and Wilson, 2007; Forlani et al., 2003; Koch et al., 2017; Tzouanacou et al., 2009). All three populations, endoderm, NotoPs and NMPs, have been reported to emerge at around mid-gastrulation (Ang and Rossant, 1994; Cambray and Wilson, 2002; Pour et al., 2022; Scheibner et al., 2021; Sulik et al., 1994; Yamanaka et al., 2007), eventually forming a progenitor zone organised along the antero-posterior axis of the embryo. On the anterior side, endodermal progenitors undergo partial EMT and intercalate into the underlying visceral endoderm to form the gut endoderm (Kwon et al., 2008; Scheibner et al., 2021; Viotti et al., 2014). NotoPs establish the ventral epithelial layer of the node, demarcating the rostral and caudal regions of the embryo (Bakker et al., 2016; Kinder et al., 2001). Finally, NMPs populate the space directly adjacent and posterior to the node and together with NotoPs form the progenitor growth zone that fuels axial

elongation (Fig 1A) (Abdelkhalek et al., 2004; Wymeersch et al., 2019). How the patterning and balanced proportion of these populations is established is not understood.

Here, we set out to identify the signalling requirements distinguishing human NotoPs from the definitive endoderm and NMPs. To tackle this challenge and circumvent the technical and ethical limitations inherent to research on rare embryonic cell populations, we have developed a tractable in vitro system that uses micropatterning to guide the development of human ESCs into reproducible patterns of notochord markers and all the lineages that surround the emergence of NotoPs. Using this system, we demonstrate that the temporal sequence of NODAL and WNT signal plays a crucial role in defining NotoPs. While strong and sustained NODAL signalling defines the definitive endoderm, NotoPs specification requires instead a transient exposure to NODAL followed by a sharp inhibition of the pathway. Our work provides insights into the earliest steps that define the axial progenitor niche and may inform the development of future strategies aimed at deriving bona-fide NotoPs from hESC.

Results

hESC colony confinement and size define cell fate patterning and axial growth

In order to study the mechanisms underlying NotoPs specification in a human context, we set out to establish an *in vitro* system that would mimic aspects of the formation of the axial progenitor zone using hESC.

Retrospective clonal analysis in mouse embryos suggest that NMPs and NotoPs may share a common ancestor (Tzouanacou et al., 2009). Furthermore, scRNAseq analysis have shown that in vitro derived NMPs contain a rare population of cells with a node-like signature (Edri et al., 2019). For these reasons, we decided to use the chemical environment of an established NMP derivation protocol as a starting point consisting of N2B27 medium supplemented with 20ng/ml of FGF2 and 2µM of the GSK3b inhibitor CHIR99021 (CHIR) which stimulates the canonical WNT pathway (Gouti et al., 2014; Tsakiridis et al., 2014; Turner et al., 2014). Given that NotoPs emerge in close proximity to NMPs within a small, confined region of the embryo (Cambray and Wilson, 2007), we hypothesised that combining an NMP derivation medium with geometrical confinement (Blin, 2021) would elicit the self-organisation of hESC colonies into standardised domains of APS cell fates including NotoPs (Fig 1B)

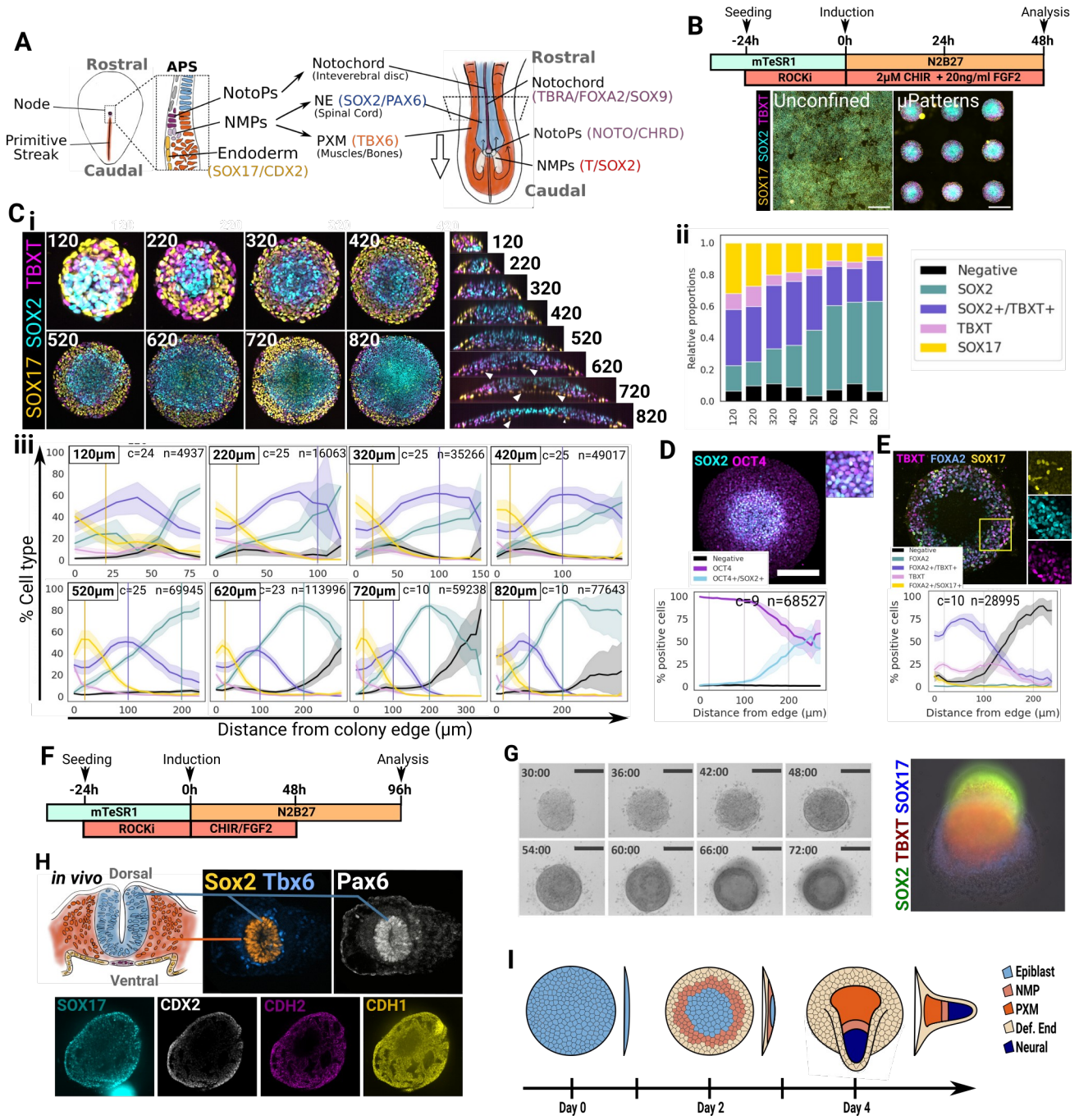

Figure 1 Geometrical confinement defines the patterning of APS cell fates in hESC colonies ***A*** *Diagram representing the human embryo at the end of gastrulation (left) and during axial elongation (right). Relevant cell lineages are indicated together with the associated cell fate markers used in this study. Extra-embryonic structures are omitted and only the posterior axis is represented on the right.* ***B*** *Illustration of the protocol used in C to E (Top) and micrograph images showing unconstrained and micropatterned cultures (Bottom). Scale bar: 500µm.* ***C*** *(i) Confocal max projections of micropatterned colonies of increasing diameters (indicated in the top left corner in µm) and stained for SOX17, SOX2 and TBXT. The corresponding Z projections are shown on the right with white arrowheads pointing at*

SOX17+ cells lining the central domain at the bottom of the colony. (ii) Stacked bar plot showing the relative proportions of individual cell populations found for each colony diameter. The number of colonies and nuclei analysed for this plot are the same as in iii. (iii) Line plots showing the mean proportion of each cell population as a function of the radial distance from the edge of the colonies. c: number of analysed colonies, n: number of analysed nuclei, shaded area: 95% confidence interval. ***D, E*** *Same as in C with 520µm colonies analysed at 48h and stained for distinct markers. scale bar: 200µm.* ***F*** *Illustration of the protocol used in G and H.* ***G*** *Selected time points from a time lapse experiment showing the development of a 320µm colony (Left). Time is indicated in hours. (Right) Widefield image of a colony stained at 96h post-induction.* ***H*** *Confocal images of 96h colonies stained for NE, PXM and endodermal markers. A diagram of a transverse view of the elongating embryo is included to illustrate the similarities.* ***I*** *Summary diagram showing the development of hAXIOMs. APS: anterior primitive streak, NotoP: Notochord Progenitors, NMPs: Neuromesodermal progenitors. NE: Neurectoderm, PXM: paraxial mesoderm.*

We first tested a range of colony diameters to determine how colony size may impact the patterning and proportions of cell fates (Figure 1C i). We stained the cells 48h post-induction for the NMP markers TBXT and SOX2 and for the endodermal marker SOX17 (Kanai-Azuma et al., 2002; Viotti et al., 2014) which we used in the first instance as a proxy for the emergence of additional APS cell fates that do not normally appear in NMP differentiation monolayers (Frith and Tsakiridis, 2019). When cells are cultured in conventional tissue culture dishes, CHIR and FGF treatment generates around 90% of cells co-expressing TBXT and SOX2 (Frith et al., 2018; Gouti et al., 2014). In sharp contrast, we observed a consistent and robust radial organisation of the tested cell fate markers for all colony sizes on micropatterns, with a T/SOX2 domain located in between a SOX2 only domain in the centre and a SOX17 domain at the periphery. Interestingly, the cells adopted a three dimensional epithelial organisation that became more apparent with increasing micropattern size. While SOX17+ cells were abundant at the periphery, these cells also formed a sparse epithelial layer lining the entire bottom of the colony, perhaps reflecting the behaviour of the nascent endoderm in vivo which undergoes partial EMT as it segregates from the mesoderm to form the gut endoderm epithelium during gastrulation (Kwon et al., 2008; Scheibner et al., 2021; Viotti et al., 2014).

Using our established single-cell-resolution quantitative immunofluorescence pipeline (Blin et al., 2019; Wisniewski et al., 2019), we measured the proportion of each individual population (Figure 1Cii). We found that increasing colony size, increased the proportion of the SOX2+ cells at the expense of the TBXT+ and SOX17+ cells (Fig1Cii). We also observed that the proportion of TBXT/SOX2 double positive cells was maximised within colonies of intermediate sizes between 320 and 520µm in

diameter. We next plotted the proportion of these populations as a function of the radial distance from the colony edge (Fig1Ciii) and found that each individual domain was located at a consistent distance from the colony edge across all colony diameters except for colonies below 320µM where this rule did not apply as strictly. These observations may suggest that the mechanisms driving the radial organisation of the cells in this context is boundary-driven as reported in other micropatterned colony systems (Etoc et al., 2016; Martyn et al., 2019; Warmflash et al., 2014). For the subsequent experiments, we decided to use 520µm colonies because this diameter offered a good compromise for analysis and imaging with a clear radial fate marker distribution.

We next asked about the developmental state of the cells forming the central SOX2 domain. SOX2 is initially co-expressed with OCT4 in the pluripotent epiblast and remains expressed in the developing neurectoderm while OCT4 becomes progressively lost as the cells exit pluripotency (Avilion et al., 2003; Osorno et al., 2012). We found that the SOX2 domain was still OCT4+ at this stage indicating that the cells had not yet exited pluripotency at the centre consistently with the notion that differentiation commences at the edge on micropatterns (Fig1D).

Next, we tested for the presence of NotoPs. We first looked for the co-expression of FOXA2 and TBXT which are both essential for the development of the notochord (Ang and Rossant, 1994; Lolas et al., 2014; Tamplin et al., 2011; Yamanaka et al., 2007) and found that a majority of TBXT expressing cells also co-expressed FOXA2 (Fig 1E). Since these markers are also transiently co-expressed in the nascent mesendoderm during gastrulation (Burtscher and Lickert, 2009), we performed FISH against NOTO transcripts which are specifically found within NotoPs (Abdelkhalek et al., 2004; Plouhinec et al., 2004). We did not observed any positive cells for this marker (not shown) suggesting that the TBXT/FOXA2+ cells represent an early APS population at this stage.

To further characterise the lineages that emerge in micropatterned colonies, we repeated the same protocol as in Fig 1B and cultured the cells for an additional 2 days in unsupplemented N2B27 (Fig 1F). Time lapse imaging revealed cell movements and growth in the central region of the colonies from 36h onwards and the emergence of an elongated structure that became apparent at around 60h post-induction (Fig 1G). At 96h, the colonies adopted a 3 dimensional organisation that retained the cell fate arrangements we observed at 48h with SOX17 at the bottom, SOX2 at the top and a ring of TBXT/SOX2+ cells in the middle (Fig 1G). Remarkably, staining for the neurectodermal marker PAX6 and the presomitic marker TBX6 revealed a multi-tissue organisation resembling the axis of the elongating embryo with SOX2 and PAX6 found co-expressed in a neural tube-like structure flanked by a few TBX6 positive cells (Fig 1H), indicating the presence of bona-fide NMPs in this system.

We were unable to find evidence of notochord-like cells co-expressing TBXT, FOXA2 and SOX9 which is normally found in the notochord (Bagheri-Fam et al., 2006), confirming that the T/FOXA2+ population identified at 48h failed to engage in the notochord lineage. On the other hand, colonies contained an abundance of FOXA2 single positive as well as an epithelial layer reminiscent of the gut endoderm marked by SOX17, CDX2, CDH1 and CDH2 (Fig 1H). These observations confirmed that confinement directs a significant proportion of the cells towards the endoderm lineage.

Altogether, these initial experiments allowed us to establish an *in vitro* system where hESC organise into reproducible and standardised domains of cell fates which further undergo morphogenetic aspects of the onset of axial elongation (Fig 1I). We decided to name this system hAXIOMs for human axis on micropatterns. While this system provides a good starting point, we were unable to detect NotoPs in these conditions, raising the question of which additional signals might be required to generate this cell type. Furthermore, we observed a decrease in NMPs proportion over time in favour of the emergence of posterior endoderm suggesting that confinement potentiates endogenous cues that deflect the cells from axial cell fates towards the posterior endoderm lineage.

2- Dynamics of NODAL, WNT and BMP signalling correlate with the loss of axial cell fates and the emergence of definitive endoderm and lateral plate mesoderm

To gain insights into the mechanisms driving cell fate diversification and the loss of axial lineages on micropatterns, we performed time course experiments and bulk RNA Nanostring analysis. We used a panel of probes consisting of the 780 genes included in the standard human embryonic stem cell gene panel together with 30 additional custom probes (listed in Table 1). This panel covered a wide array of genes involved in differentiation, metabolism, signalling pathways and the cell cycle. In order to analyse our dataset, we used the Bioconductor package moanin (Varoquaux and Purdom, 2020) which allowed us to group individual genes based on their temporal profile (see Methods). We identified 7 clusters that are shown in Fig2A. Cluster 1 and 2 identify genes that are expressed at the start and then progressively downregulated. As expected, these include pluripotency markers such as MYC, OCT4, DPPA4, DNMT3B and ZFP42. We found NANOG to be highest at around 36h and then lost rapidly consistently with the fact that Nanog is re-expressed in the posterior epiblast at the onset of gastrulation *in vivo* (C et al., 2018; Hart et al., 2004; Osorno et al., 2012). We also found SOX2 in cluster 2 as a gene that is rapidly downregulated and starts to re-emerge at around 72h most likely as a result of its expression in the central domain undergoing neural differentiation (Fig1H).

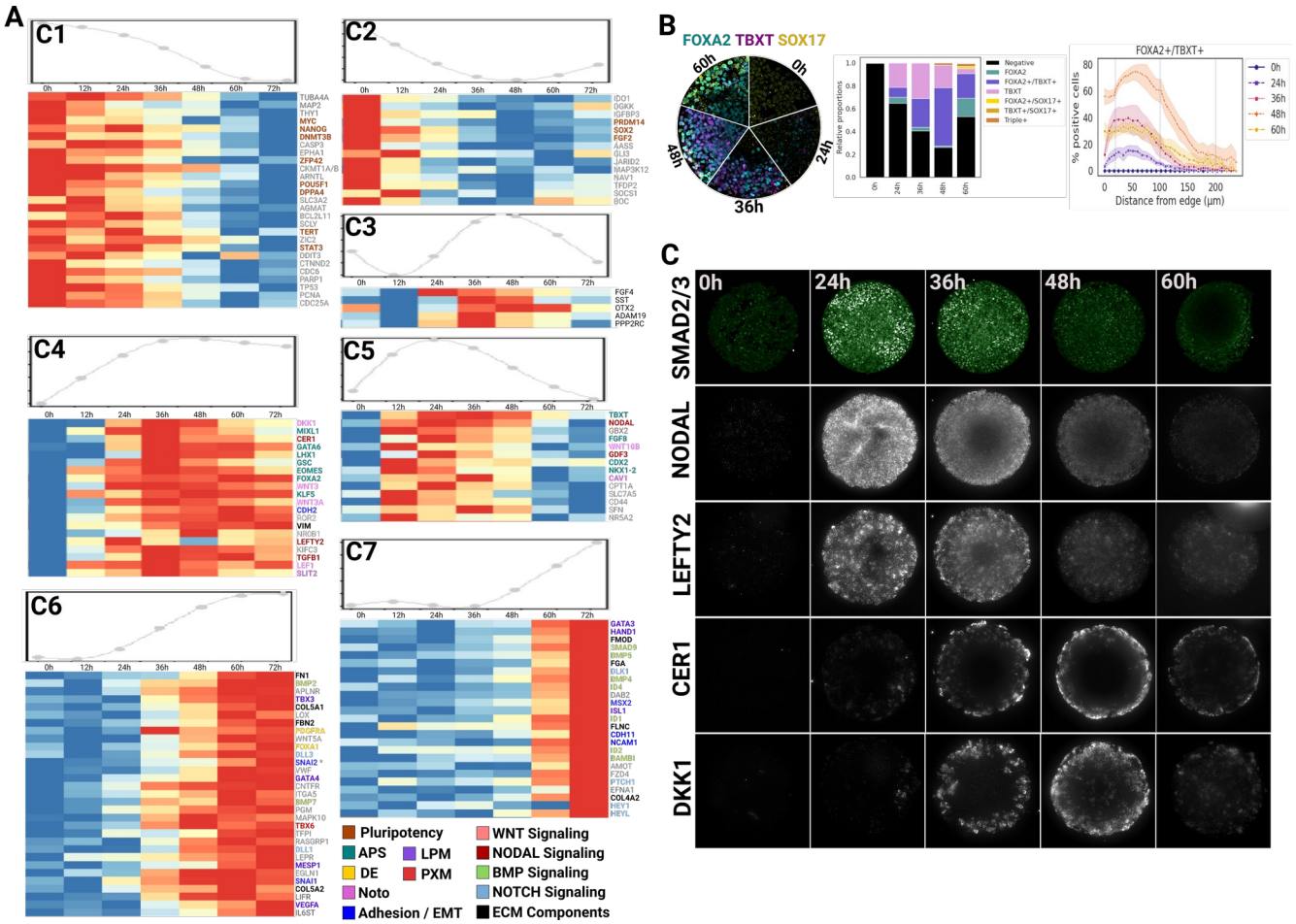

Fig 2 Dynamics of NODAL, WNT and BMP signalling correlate with the loss of axial cell fates and the emergence of definitive endoderm and lateral plate mesoderm - ***A*** *Nanostring time course analysis. Cells were treated as in Fig. 1F. For each cluster, the figure includes the model spline of the cluster (top) and a heatmap showing the scaled level of expression of the genes. Genes are ordered in decreasing order of maximum differential expression amplitude from top to bottom.* ***B*** *quantitative immunofluorescence time course analysis of the expression of FOXA2, TBXT and SOX17 in 520µm colonies. Left: confocal max projections, Middle: stacked bar plot showing the relative proportions of individual cell populations over time, right: line plots showing the mean proportion of the FOXA2/TBXT double positive population over time as a function of the radial distance from the edge of the colonies. c: number of analysed colonies, n: number of analysed nuclei, shaded area: 95% confidence interval.* ***C*** *Immunofluorescence (SMAD2/3) and branched FISH (other markers) images of 520µm colonies at selected time points during the first 60h of hAXIOMs development.*

Cluster 4 and 5 identified genes that become expressed as early as 12h post-induction with Cluster 4 regrouping genes with a sustained expression after 36h while cluster 5 includes genes that peak at 36h and then decrease. These 2 clusters revealed a clear APS signature with the expression of MIXL1 (Hart et al., 2002), LHX1 (Costello et al., 2015), EOMES (Costello et al., 2011), GSC, CDX2, FOXA2 (Burtscher and Lickert, 2009), KLF5 (Aksoy et al., 2014) as well as the NMP-associated gene NKX1-2 (Albors et al., 2018). Encouragingly we also found a peak of expression of the notochord markers SLIT2 and CAV1 (Fang et al., 2006) at 36h. However, NMPs and NotoPs associated genes decreased over time indicating that axial progenitors became rapidly depleted. We confirmed this using quantitative immunofluorescence and observed that while the majority of the cells expressed TBXT/SOX2 at 24h, these markers were progressively lost in favour of SOX17 (Sup Fig1A). Similarly more than 50% of the cells co-expressed TBXT and FOXA2 at 48h but this population was more than halved 12h later with a significant fraction of the FOXA2+ cells gaining SOX17 expression (Fig2B and Sup Fig1B) suggesting that some of these cells were on their way to form endoderm.

In fact, many of the genes found in cluster 4 and 5 of our Nanostring dataset are known regulators of the endodermal lineage. For example, both MIXL1 and KLF5 are required for specification of the definitive endoderm (Aksoy et al., 2014; Hart et al., 2002; Moore-Scott et al., 2007) and LHX1, while expressed in the node, works together with OTX2 (found expressed transiently in cluster 3) to define anterior endoderm (Costello et al., 2015). Furthermore, looking at cluster 6 and 7, where genes become upregulated from 48h onwards, we could confirm the emergence of additional endodermal markers such as FOXA1 (Ang and Rossant, 1994), PDGFRA and GATA4 as well as several ECM components some of which likely secreted by the endoderm including FN1, COL4A2, COL5A1, COL5A2, FBN2 and FLNC.

Importantly, endoderm was not the only lineage emerging in our colonies as we could observe clear evidence of lateral plate mesoderm specification. GATA6 (Morrisey et al., 1996; Zhao et al., 2005) and EOMES (Costello et al., 2011), found in cluster 4, are both involved in the specification of the endoderm and the cardiac mesoderm lineage in the streak, and cluster 6 and 7 regrouped many genes associated with the lateral plate mesoderm including GATA3, HAND1, ISL1, TBX3 (Washkowitz et al., 2012) and MESP1 alongside the EMT markers SLUG, SNAIL and MSX2. Lineage tracing experiments in mice have shown that cardiac precursors are specified early in the streak from a population of cells that transiently express FOXA2 (Bardot et al., 2017). It is therefore possible that the fraction of FOXA2+ cells that does not turn SOX17 on (Fig 2I) is instead producing cardiac mesoderm in addition to definitive and anterior endoderm.

Overall, these observations show that cells on micropatterns follow a coherent developmental program. However, while the cells initially follow the route towards axial cell fates (i.e express APS

markers), the cells are eventually deflected towards other lineages including endoderm and lateral plate mesoderm.

We thus turned our focus towards endogenous signalling pathways that may explain the observed endoderm and mesoderm differentiation. NODAL is a known driver of mesodermal and endodermal specification (Robertson, 2014) and its expression is positively regulated by the canonical WNT pathway (Ben-Haim et al., 2006; Norris et al., 2002); a pathway that we stimulate with CHIR in our cultures. Our Nanostring data showed upregulation and sustained expression of the WNT target gene LEF1 (Cadigan and Waterman, 2012) as early as 12h while NODAL expression peaked at 24h before decreasing progressively (FIG 2A). This peak of NODAL was followed by a peak of CER1 expression at 36h. FISH confirmed the temporal expression profile of NODAL and CER1 (Fig2 C). Interestingly NODAL expression was widespread across the colony at 24h and so was its antagonist LEFTY2. On the other hand, we only detected nuclear expression of the NODAL pathway effector SMAD2/3 in the peripheral region of 24h colonies, further confirming that a spatial pattern of responsiveness to NODAL exist in the colonies. This region matched spatially and preceded temporally the domain of APS markers emergence (see TBXT/FOXA2 in Fig2B) where CER1 (Belo et al., 1997; Perea-Gomez et al., 2002) and the WNT antagonist DKK1 (Semënov et al., 2001) were also found (Fig2 D).

Altogether, our data revealed the implementation of a regulatory network of signalling molecules in hAXIOMs involving WNT, NODAL and their respective inhibitors suggesting that these pathways are responsible for the loss of axial fate markers and the emergence of both definitive endoderm and lateral plate mesodermal lineages.

3- A non-linear interaction between WNT and NODAL signalling dictates APS cell fate patterning in hAXIOMs

Our findings suggested that the balance between WNT and NODAL regulate the balance of APS cell fates in hAXIOMs and could be central to specifying NotoPs. To test this, we next decided to manipulate the levels of these pathways. We first tested a range of CHIR concentrations and monitored markers of cell fates 48h post-induction (FIG 3A). In the absence of CHIR, all the cells remained OCT4/SOX2 double positive and negative for TBXT, FOXA2 (Sup Fig2 A and B) and SOX17 (FIG 3A) showing that exogenous stimulation of the WNT pathway is required to initiate differentiation. More importantly, we found a clear dose-dependent effect of CHIR on the levels and spatial distribution of cell fate markers: The percentage of SOX2+ cells was negatively correlated to CHIR concentration while the percentage of TBXT+ cells increased proportionally in line with the fact that

TBXT is a known direct target of the WNT/β-catenin pathway (Arnold et al., 2000). On the other hand, SOX17 and FOXA2 did not correlate linearly with CHIR levels. Instead, both SOX17 and FOXA2 emerged at intermediate concentrations and were rare or absent at higher concentrations (FIG3A and Sup Fig2 C), showing that high WNT pathway activity is incompatible with endoderm differentiation on micropatterns.

Interestingly, when considering the spatial distribution of these markers, we observed a clear inward shift of the different cell populations when CHIR was increased (FIG 3A iii):
TBXT was expressed at the periphery with 1µM CHIR and progressively expressed throughout the colony with increasing concentrations. In parallel, SOX2 was downregulated at the periphery with 2µM CHIR and higher concentrations were required to repress SOX2 in the centre. As a result, TBXT/SOX2 double positive cells were found at the periphery at 1µM CHIR but were progressively shifted and restricted to the centre, forming a smaller fraction of the total population with increasing CHIR concentration where TBXT single positive cells became predominant. Finally, SOX17 appeared restricted at the edge at 1µM CHIR, but spanned a 150 µm domain at 2µM, while at 3µM, the few SOX17+ cells present in the colony were located at around 100µm from the border (FIG 3A iii – yellow line). Together, these observations further support the idea that CHIR-induced patterning is initiated from the periphery of the colony. Importantly, this experiment also show a complex, non-linear dose-dependent action of CHIR on cell fates. Since CHIR induces NODAL (Fig 2; see also (Martyn et al., 2018; Massey et al., 2019), and the dynamics of NODAL and WNT activity is understood to dictate cell fates (Chhabra et al., 2019; Heemskerk, 2019; Yoney et al., 2018), our results raise the possibility of a non-linear effect of CHIR concentration on NODAL expression which would in turn define cell fate outcomes on micropatterns.

To test this idea, we next performed FISH against NODAL transcripts across the same range of CHIR concentrations (Fig 3B). Strikingly, NODAL was expressed exclusively at the extreme periphery of the colony at 1µM CHIR and was broadly expanded at 2µM CHIR. This pattern of expression overlapped closely to the positioning of the SOX17+ cells found in Fig3A, further supporting the idea that CHIR-driven NODAL induction is responsible for the emergence of the definitive endoderm in hAXIOMs. Importantly, while NODAL expression became stronger and broader up to 2µM of CHIR, higher concentrations resulted in a decrease in NODAL expression where endoderm was reduced or absent and mesoderm predominated. These results confirm the non-linear dependence of NODAL expression to CHIR dosage and while it is possible that a strong induction of NODAL exists at earlier time points, these observations also suggest that long or strong exposure to NODAL induces endoderm while a short or low exposure may be needed for mesoderm induction.

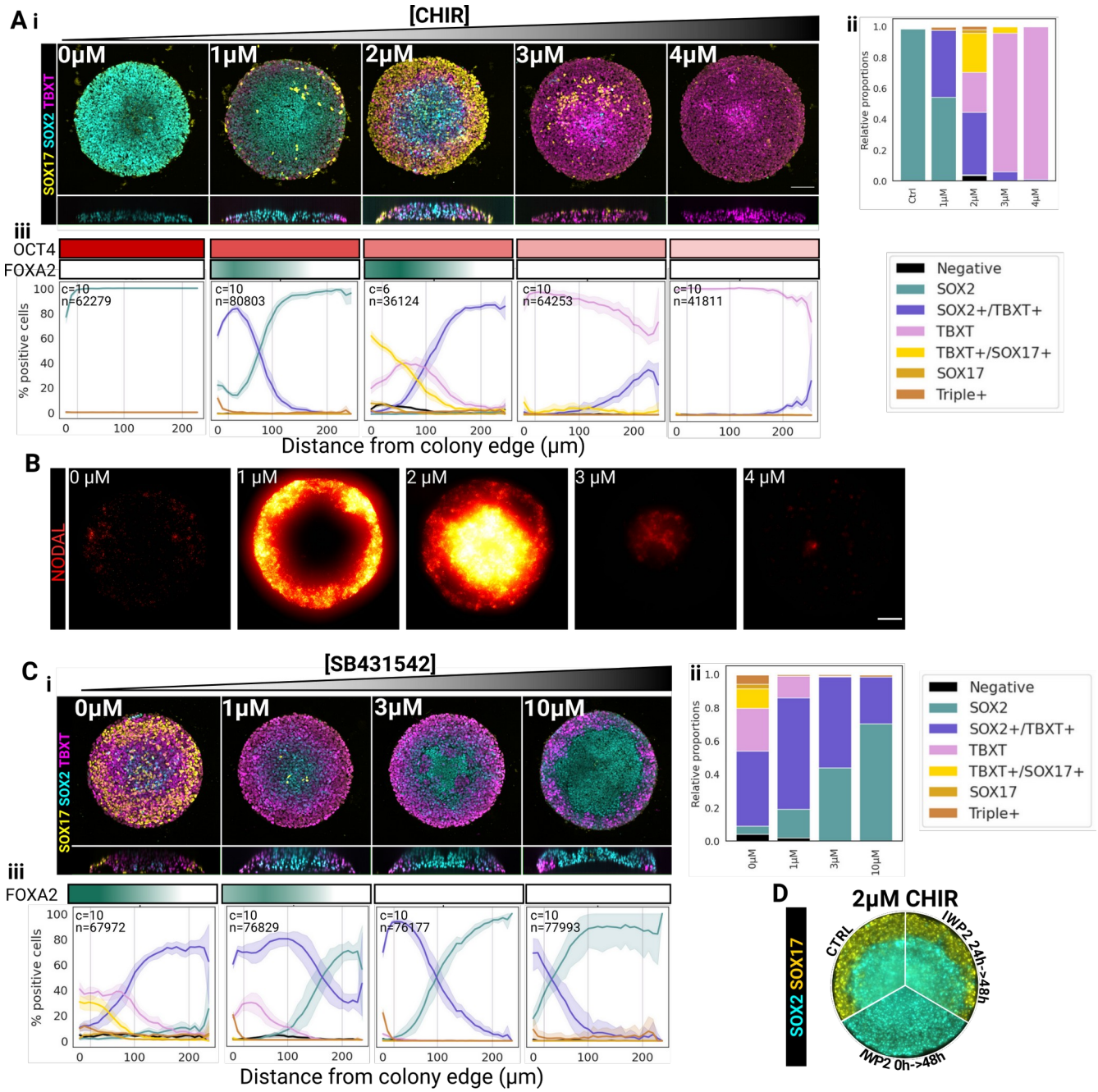

Fig 3 A non-linear interaction between WNT and NODAL signalling dictates APS cell fate patterning in hAXIOMs - ***A*** *CHIR dose response in 500μm colonies fixed at 48h. (i) Images show the max projections of confocal z stacks (top) and a z projection (bottom). (ii) Stacked bar plot showing the relative proportions of individual cell populations for each CHIR concentration. (iii) Radial profile of the percentage of each population. Note that OCT4 and FOXA2 are indicated as colour bars based on the data supplied in Sup fig 2A and B while SOX2, SOX17 and TBXT are shown as line plots. c: number of analysed colonies, n: number of analysed nuclei, shaded area: 95% confidence interval.* ***B*** *Branched FISH analysis of NODAL expression upon increasing amounts of CHIR (concentrations indicated in white). Images show a representative max projection of a widefield z stack.* ***C*** *SB435192*

dose response in 500µm colonies treated with 2µM CHIR and FGF and fixed at 48h. Images and plots as in (see also Sup Fig 3 for the full details of the FOXA2 profile of expression). ***D*** *IWP2 response in 520µm colonies treated with 2µM CHIR and FGF and fixed at 48h.*

To confirm this hypothesis, we next decided to titrate NODAL activity using varying doses of the TGFβ/NODAL receptors inhibitor SB431542 (Inman et al., 2002) (Fig3C). We observed that even low amounts of SB431542 was sufficient to strongly reduce the proportion of SOX17 positive cells confirming that high NODAL signalling activity is indeed required for endoderm specification (Fig3Ci - 1µM). In line with previous findings showing that APS fates can emerge when NODAL levels are reduced (Plouhinec et al., 2022), FOXA2 remained expressed at $1\mu M$ SB (Fig3Ci colour bar and Sup Fig 2B) indicating that the cells were either slower to progress along the endodermal lineage or that they were adopting a distinct fate. Remarkably, increasing the dose of NODAL inhibitor progressively expanded the central domain of SOX2 single positive cells at the expense of the TBXT/SOX2 double positive cells which became more and more restricted to the periphery (Fig 3C). These results show that artificially decreasing the cells responsiveness to NODAL reduces the proportion of cells undergoing mesodermal or neuromesodermal specification thus confirming that low or short NODAL exposure is necessary to induce TBXT expression in this context.

Finally, since our Nanostring results in Fig 2 show that CHIR induces WNT ligands as well as NODAL expression, we decided to test the role of endogenous WNT. To do so, we treated the cells with the porcupine inhibitor IWP2 which blocks the secretion of WNT molecules (Chen et al., 2009) (Fig 3D). We did this at 2µM IWP2 concentration where all markers were previously observed. To our surprise, IWP2 treatment for the whole 48h resulted in the complete loss of SOX17 indicating that endogenous WNT is required to induce endoderm. On the other hand, IWP2 treatment for the last 24h had little effect suggesting that WNT ligand exposure is required early and is dispensable after 24h. These results are in line with previous work showing that WNT priming is required prior NODAL exposure to induce endoderm (Yoney et al., 2018; Yoney et al., 2022). However, our data also raise the question as to why isn't CHIR exposure sufficient to accomplish this priming. Previous work has shown that CHIR induces distinct transcriptional dynamics than WNT ligands (Massey et al., 2019), it will be interesting to elucidate in future whether this might explain the effect that we observe here.

In summary, our results demonstrate that even very small variations in CHIR concentration induce distinct NODAL expression levels and dynamics which in turn determines the choice of endoderm or mesoderm fate. Strong sustained NODAL specifies endoderm, while weak transient NODAL induces mesoderm. We also uncover an unexpected early requirement for endogenous WNT ligands in endoderm specification even in the presence of the GSK3β inhibitor. All together, these experiments

allowed us to gain insights into the mechanisms driving fate patterning in hAXIOMs and begin to characterise a system that will be useful for more detailed mechanistic studies in the future.

4- Abrupt Nodal inhibition is required for the spontaneous emergence of NotoPs in hAXIOMs

We next turned to the question of how to further modify signalling in order to achieve NotoP differentiation. Specification of NotoPs requires the cooperation of WNT and NODAL signals in the mouse embryo (Lickert et al., 2002; Vincent et al., 2003; Yamamoto et al., 2001). However, our previous results show that varying WNT activity alone is not sufficient to elicit NotoPs in hAXIOMs despite the consequences of WNT activity on downstream NODAL signalling. We also observed that titration of endogenous NODAL activity could balance endoderm and mesoderm but failed to induce NotoPs. Given these considerations, we hypothesised that the NODAL signalling dynamics established spontaneously within our colonies is inadequate for NotoPs emergence and that a tight exogenous control of NODAL dynamic together with sustained WNT activity is instead necessary.

To test this hypothesis, we inhibited NODAL after 24h of CHIR/FGF induction, at the time of peak NODAL induction and just prior to the decrease in expression of the notochord makers SLIT2 and CAV1 found in our Nanostring analysis (Fig 2). Since BMP signalling has also been shown to inhibit specification of the notochord (Yasuo and Lemaire, 2001) and that we found BMP2 expression initiated around 24h-36h (Fig 2), we also included conditions with the BMP inhibitor LDN (Fig 4A).
As expected, we observed high NODAL expression and an absence of NOTO signal in the control. Interestingly, we found a broad domain of CHRD transcripts across the colony, a BMP inhibitor expressed in the APS and rapidly restricted to the node (Bachiller et al., 2000). It is possible that CHRD in this condition was expressed in the cells transiting through an early APS mesendoderm state. LDN treatment for the entire duration of the experiment had no effect on either of the markers. SB treatment from 0h abolished NODAL expression and strongly reduced CHRD expression. This treatment also resulted in the presence of rare NOTO/CHRD double positive cells at the periphery of the colony, indicating that some NotoPs can be specified in this condition.

Strikingly, NODAL inhibition from 24h onwards induced a large domain of strong NOTO and CHRD co-expression localised at the periphery. This effect was highly reproducible across all colonies within the experiment (Sup Fig 4). Addition of LDN at 24h further potentiated this effect confirming that BMP signalling inhibits NotoPs specification.

To further confirm these results we maintained the cells for an additional 2 days in unsupplemented medium with or without SB added at 24h (Fig 4B). We next stained the cells for FOXA2 and SOX9

which likely mark NotoPs based on our observation that they are co-expressed in the node's crown cells and the nascent notochord in early bud mouse embryos (Fig 4C). While SOX9 was absent from FOXA2 expressing cells in the control colonies, we found a significant number of FOXA2 and SOX9 double positive cells when SB was added at 24h. This provides evidence that delayed NODAL inhibition in hAXIOMs produces notochord-competent NotoPs.

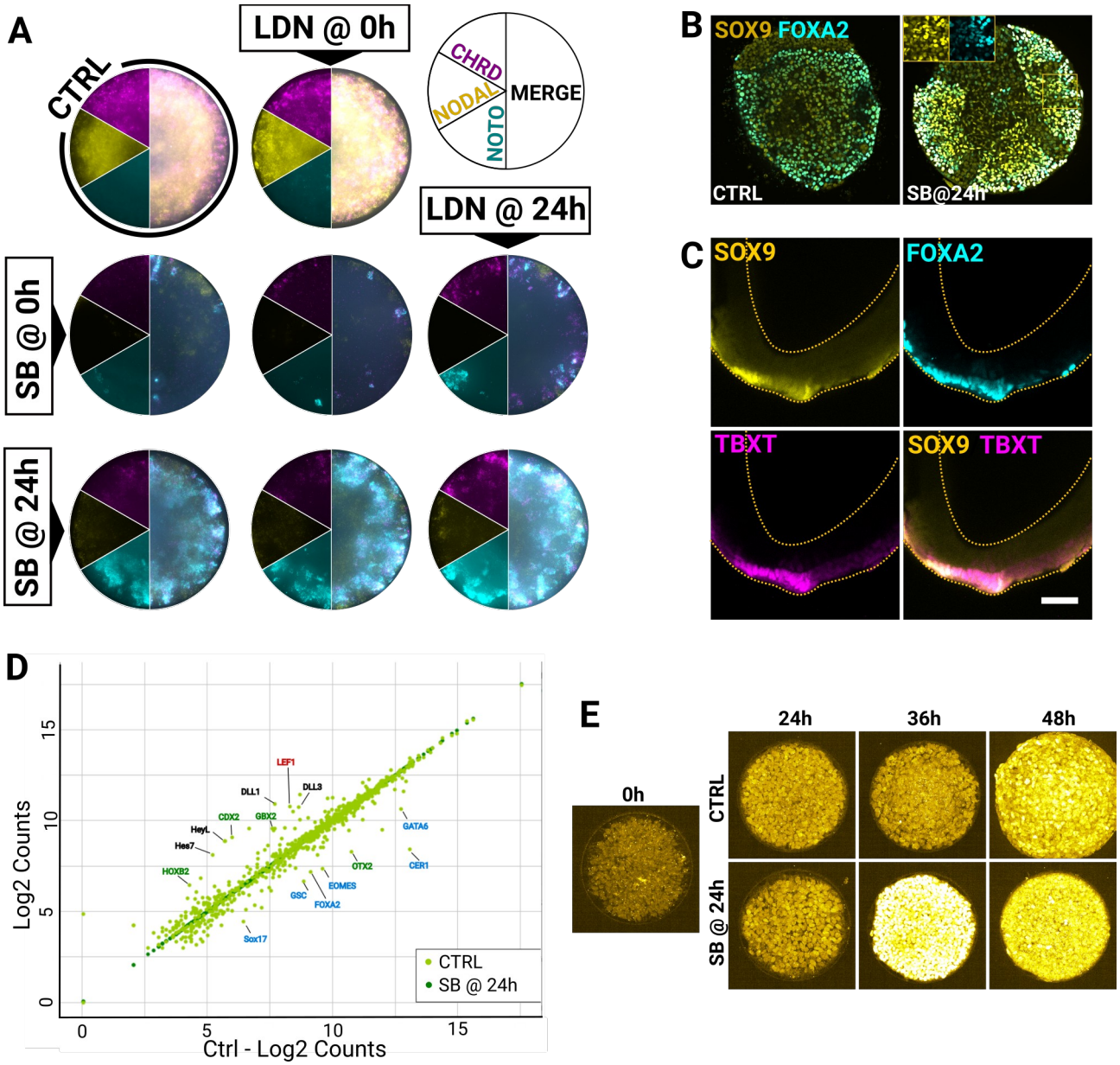

Fig 4 Abrupt Nodal inhibition is required for the spontaneous emergence of NotoPs in hAXIOMs - ***A*** *FISH staining for NODAL, CHRD and NOTO in 520µm micropattern colonies induced with 2µM CHIR and 20ng/ml FGF2 and fixed at 48h post induction. Timed treatment with the Nodal or BMP inhibitors are indicated.* ***B*** *Confocal images of micropatterned colonies cultured as in A for an*

additional 2 days with or without SB added at 24h, fixed at 96h and stained for TBXT and FOXA2. ***C*** *TBXT/FOXA2/SOX9 triple staining in early bud mouse embryo. Notice the SOX9 expression in the crown cells of the node and the nascent notochord. Scale bar: 100µm.* ***D*** *Nanostring gene expression profile comparison of micropatterned colonies at 48h with or without Nodal inhibition at 24h.* ***E*** *LEF1 staining in 320µM colonies at 24h, 36h and 48h post induction with or without SB treatment at 24h post induction.*

We next set out to understand the changes in signalling downstream of NODAL inhibition which might explain the specification of NotoPs. We used Nanostring to find differentially expressed genes in 48h colonies with or without the NODAL inhibitor SB added at 24h (Fig 4D). Interestingly, we observed the upregulation of several NOTCH signalling related genes when NODAL was inhibited at 24h as well as genes indicating a more anterior identity such as GBX2 and HOXB2. Importantly, we also found a strong increase in the WNT target gene LEF1. We confirmed this result by immunofluorescence and indeed found higher levels of LEF1 expression 12h after SB addition compared to the control (Fig 4E) suggesting that NODAL inhibition may potentiate the cells responsiveness to canonical WNT signalling.

Together our data clarify how WNT and NODAL signalling cooperate in order to specify the notochordal lineage. While WNT and NODAL signalling are initially necessary to induce an early APS cell state, a timely and abrupt inhibition of NODAL signalling is necessary to define NotoPs. Our data also show that geometrical confinement together with timely NODAL inhibition enables the efficient, reproducible and spatially organised emergence of NotoPs.

Discussion

The series of lineage restrictions that occur in the APS during gastrulation remain challenging to investigate in vivo and this is especially true in a human context. Here we have established a simple culture system that enables us to direct hESC into reproducible and standardised patterns of all the APS cell fates including NotoPs (Fig 5), a population of progenitors that has long been difficult to obtain in vitro (Colombier et al., 2020).

We have first shown that hESCs confined on micropatterns follow a coherent developmental program upon stimulation with CHIR and FGF (Fig 1 and 2). We showed that within 48h of induction, the cells establish an APS-like region that spans a 200µm domain along the periphery of the colony and then

go on to initiate aspects of axial elongation to form a multi-tissue architecture resembling the posterior region of the elongating embryo (Fig 1 F-I). This system complements previously established 3D models of axial elongation (Beccari et al., 2018; Martins et al., 2020; Moris et al., 2020; Olmsted and Paluh, 2021; Sanaki-Matsumiya et al., 2022; Turner et al., 2017; Veenvliet et al., 2020). 3D models harbour remarkable levels of organisation that beautifully mimic the developmental stages that come after the establishment of the axial progenitor niche. In comparison, hAXIOMs harbour a limited elongation, at least in the absence of NODAL inhibition. However, the patterning that precedes elongation in hAXIOMs is easy to image, highly reproducible and the orientation of the symmetry breaking event that defines the direction of axis growth is fixed in space and predictable. hAXIOMs are therefore specifically well suited to study the patterning events that precede and initiate axial elongation. Here we have exploited hAXIOMs advantages to identify the path to notochord progenitors and on this journey, delineated the signalling sequences that segregate individual APS cell fates from one another (Fig 5).

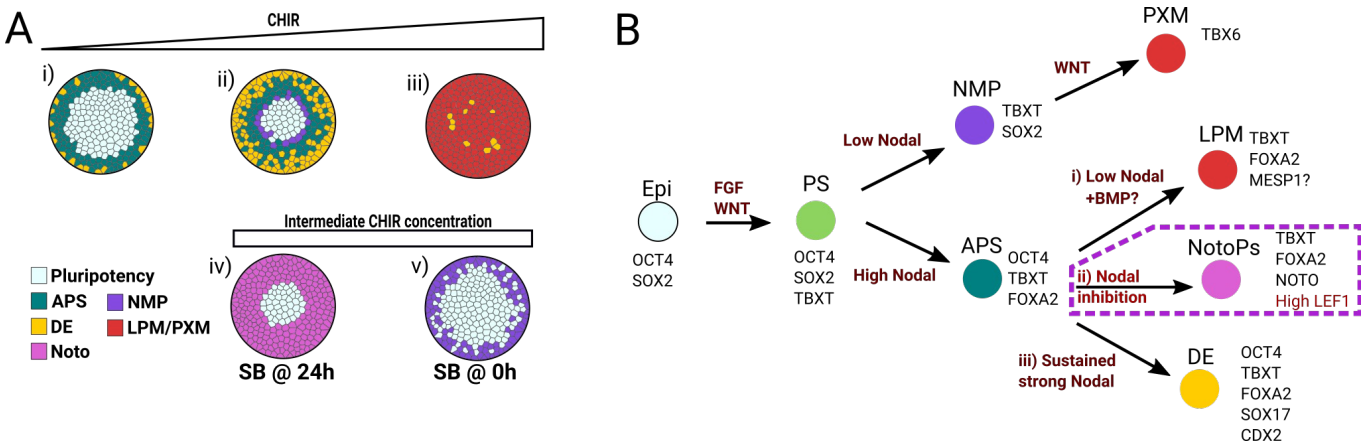

Fig 5 hAXIOMs as a model system to understand the lineage restrictions of the APS - ***A*** *Diagram summarising the spatial organisation of APS cell fates in hAXIOMs and the conditions enabling a shift in the balance of fates. All represented conditions are for 520µm colonies at 48h post-induction with CHIR and FGF. (i) low CHIR concentrations induce a minimal amount of APS markers at the edge while the pluripotent domain predominates eventually giving rise to neurectoderm (ii), intermediate CHIR enables the radial patterning of DE, early APS, NMP and epiblast with the highest proportion of DE amongst all conditions. (iii) The highest levels of CHIR lead the majority of the cells differentiating to mesodermal fates. (iv) NotoPs can be obtained with intermediate CHIR levels and an inhibition of NODAL signalling 24h post-induction.* ***B*** *Hierarchy of lineage restrictions and signalling defining cell fate bifurcations. The epiblast (Epi, expressing OCT4 and SOX2) differentiate over time into primitive streak fates (PS, expressing OCT4, SOX2, and TBXT) which then depending on the Nodal response can give rise to either neuromesodermal progenitors (NMP, expressing TBXT, SOX2) when there is low Nodal response, and broader APS fates (expressing OCT4, TBXT, FOXA2) when*

there is high Nodal response. NMPs upon WNT stimulation give rise to PXM. The APS fates can change dynamically over time depending on the treatment ***i)*** *low Nodal response and potentially BMP signalling drive lateral plate mesoderm (LPM) fate,* ***ii)*** *Nodal inhibition drives the NotoPs (notochord progenitor) fate,* ***iii)*** *sustained strong Nodal signalling drives DE fate.*

We were at first surprised by the diversity of fates that we observed on micropatterns given that the same concentration of CHIR and FGF applied to cells grown in 2D monolayer normally leads to homogenous NMP differentiation. This indicated that confinement and the boundaries imposed on colonies modified the cells response to the signalling we provided exogenously. Previous work with BMP or WNT ligands as a differentiation trigger on micropatterns has shown that confinement imposes a pre-pattern in epithelial integrity which in turn dictates the ability of the cells to respond to these signals (Etoc et al., 2016; Legier et al., 2023; Martyn et al., 2018; Martyn et al., 2019; Warmflash et al., 2014). Our data indicate that a similar mechanism is likely taking place here as well. This was indicated by the lack of scaling of the differentiation domains with increasing colony sizes (Fig 1C) and by the fact that nuclear localisation of the NODAL effector SMAD2/3 was restricted to the periphery in spite of the ubiquitous expression of NODAL transcripts throughout the colony at 24h (Fig 2C). Thus a safe assumption would be that in this system, CHIR induces NODAL in all the cells regardless of their position in the colony, and that differentiation begins at the periphery as a result of the increased responsiveness of the cells to the secondary signals induced by CHIR. This in turn would result in the cells experiencing distinct levels and duration of WNT and NODAL signalling activity according to their location relative to the periphery. Note that we have not explored the role of FGF in this study although it is possible that differential responsiveness to FGF may be involved in driving cell fates from the boundary.

Our CHIR dose-response experiment (Fig 3A) was particularly revealing and helped us to delineate the signalling sequences that segregate individual APS cell fates from one another (summarised in Fig 5). We found that even very small variations in CHIR concentration radically changed the proportion of endodermal and mesodermal cell fates. Importantly, we found that this was mediated by a non linear relationship between WNT activity and the downstream dynamics of NODAL expression (Fig3B and C). Intermediate levels of CHIR induced the highest and most sustained levels of NODAL production favouring the endodermal lineage while higher CHIR levels resulted in a sharp reduction of NODAL at 48h and an increase in BMP which correlated with an abundance of mesoderm. Our data sheds some light on how distinct signalling dynamics may be established as the cells ingress into the streak and on the specific signalling regimes associated with individual cell fates (Fig 5B):

1) We have found that NMPs require an environment where NODAL activity is maintained at a minimum (Fig 3C). This idea is compatible with the fact that NMPs ingress later than endoderm in mice, at a time when NODAL signalling activity starts to decrease (Lawson et al., 1991). Furthermore, neighbouring NotoPs - as a source of NODAL inhibitors - may protect NMPs from advert differentiation during axial elongation. Indeed a release of NODAL inhibition might explain why NotoPs ablation results in early termination of axial elongation (Abdelkhalek et al., 2004; Wymeersch et al., 2019).

2) Our observations also show that a large proportion of the cells differentiate to lateral plate mesoderm in hAXIOMs, most likely under the influence of endogenous BMP signalling (Fig 2 and 3). This is perhaps not surprising as fate mapping experiments have shown that cardiac mesoderm arise directly adjacent to the definitive endoderm (Lawson et al., 1991; Tam et al., 1997) and lineage tracing using FOXA2 cre lines have demonstrated that a proportion of FOXA2 expressing cells in the streak are fated to form cardiac ventricles (Bardot et al., 2017). It will be interesting to use hAXIOMs in the future to determine the detailed mechanisms that distinguish LPM from other transiently FOXA2+ cell types emerging in the APS.

3) Finally, our manipulations of NODAL and BMP signalling in hAXIOMs has enabled us to identify the path to the notochord lineage (Fig 4A). While prolonged NODAL exposure drives endoderm differentiation, a sharp inhibition of NODAL after an initial surge leads to the spontaneous emergence of NotoPs in hAXIOMs. This finding is consistent with observations in the xenopus where a sudden drop of p-Smad2 correlates with the emergence of the notochord (Schohl and Fagotto, 2002). Interestingly, we also found that NODAL inhibition potentiates WNT activity (Fig 4D and E). This signalling interaction may reinforce the notochord lineage as WNT signalling is known to maintain the notochord fate and support the posterior extension of the node (Ukita et al., 2009). Recent evidence support the idea that the node is formed of a heterogeneous population of cells (Rito et al., 2023), it will be interesting to test if a fully functional node can be reproduced in vitro in the future and determine what other signalling cues define the proportion and maturation of these node sub-populations.

Conclusion

NotoPs are regarded as a promising cell type for drug discovery or cell therapy and much remains to be learned about the healthy and pathological development of the notochord. Encouragingly, recent evidence suggest that NotoPs persist as a small transcriptionally stable population throughout axial elongation (Wymeersch et al., 2019) making it likely that NotoPs may be expandable in culture if the correct conditions can be identified. Our work together with the recent work from Rito and colleagues

(Rito et al., 2023) provides insights that will inform the development of reliable NotoPs derivation protocols. Furthermore, the experimental system that we introduce here should form an excellent platform to further understand the mechanisms underlying the gastrulation to axial elongation transition or as a sensitive assay to assess the differentiation phenotype of hPSC lines with distinct genetic background.

Materials and Methods

Cell culture

All experiments used the MasterShef7 hESC line obtained from the University of Sheffield. hESC were propagated at 37°C and 5% CO_2 in mTSER Plus medium (100-0276, Stemcell Technologiess) on Geltrex (A1413302, Life Technologies) coated 6-well plates (3516, Corning Incorporated). Wells were coated for 30 minutes at 37°C using a 100µg/mL Geltrex solution diluted in Magnesium and Calcium containing DPBS (14080-048, GIBCO). Passaging was performed every 2 to 3 days using Accutase (00-4555-56, ThermoFisher Scientific). The cells were Mycoplasma tested prior to running experiments. Only cells with a passage number below 30 were used for all experiments.

Micropattern fabrication

Micropatterning was done in Ibidi 8-well µSlides (IB-80826, Ibidi) with a PRIMO bioengineering plateform (Alveole) mounted on a Nikon Ti2 Widefield microscope using a protocol adapted from Alveole: The surface of ibidi slides was first passivated as follows: slides were plasma treated (Harrick Plasma Cleaner) for 1 min 30 seconds at high intensity in a 200 mTorr vacuum and then incubated at room temperature for 1h with 200µL/well of 200 µg/mL Poly-D-Lysine (A-003-E, Merck Millipore) diluted in 0.1M HEPES pH 8.4 (H3784-25G, Sigma-Aldrich). The wells were washed 3 times with 0.1M HEPES pH 8.4 and then incubated for 1h in the dark with 125µL/well of 80mg/mL mPEG-SVA (MPEG-SVA-5000, Laysan Bio) freshly dissolved in 0.1M HEPES pH 8.4. Slides were then washed profusely with ddH_2O, air dried and stored at 4°C until further processing (1 week maximum). The PRIMO insolation step was next performed less than one day prior to plating the cells: passivated wells were covered with 8µL PLPP gel (Cairn Research, 1µL PLPP gel/well diluted with 7µL 70% Ethanol) in the dark and left to dry for ~30min at room temperature. Slides were then insolated with PRIMO through a 20X lens with a dose of 50mJ/cm^2. All micropattern shapes were designed in Inkscape and converted to binary tiff files in ImageJ prior to loading in the Alveole Leonardo software. After insolation, PLPP gel was removed with 3 ddH2O washes and the slides were air dried and stored at 4°C until use.

Culture on micropatterns

Micropatterned Ibidi slides were first rehydrated for 5 min in Magnesium and Calcium containing DPBS (14080-048, GIBCO; thereafter DPBS++). Matrix coating was then performed by incubating the wells at room temperature for 30 min with a mixture of 40µg/mL rhVitronectin-N (A14700, ThermoFisher) and 10µg/mL rhLaminin521 (A29249, GIBCO) diluted in DPBS++. Wells were washed 3 times with DPBS++ and left in the last wash whilst preparing the cells for seeding to ensure that the wells were not left to dry. For seeding, 80% confluent MasterShef7 cells were dissociated to single cells with Accutase, and resuspended in seeding medium composed of mTESR Plus supplemented with 10µM Y-27632 (1254, Tocris Bio-Techne) and 1:100 Penicillin/Streptomycin (10,000U/mL pen, 10,000mg/mL strep ; 15140-122 ,Invitrogen). Cells were plated onto micropatterns at a density of 200 000 cells/well in 250µL of seeding medium. The cells were left to adhere for 3h at 37°C. After attachment, the excess of cells was removed by gentle pipetting and applying fresh seeding medium. The cells were left to settle and cover the patterns overnight until induction of differentiation the next morning. Cells were washed once in N2B27 to remove traces of growth factors present in seeding medium. Differentiation was then induced using N2B27 medium supplemented with Penicillin/Streptomycin (1:100), 2µM CHIR 99021 unless specified otherwise (4423/10, Tocris Bio-Techne), 20ng/ml human bFGF (PHG6015, ThermoFisher Scientific), 10µM SB 431542 unless specified otherwise (1614, Tocris Bio-Techne) and/or 0.1µM LDN 193189 unless specified otherwise (72147, StemCell Technologies). The medium was replaced every 24h until analysis.

Immunofluorescence

Mouse embryos were staged according to (Downs and Davies, 1993) and stained as described previously in (Wong, 2021). Cells grown on micropatterns were fixed with 4% PFA (CHE2036, Scientific Laboratory Supplies), washed 3 times with a solution of PBS and 0.1% Triton X-100 (A16046, Alfa Aesar; hereafter PBST) and left overnight at 4°C in blocking solution containing 3% Donkey Serum (D9663, Merck) and 0.03% Sodium Azide (40-2000-01, Severn Biotech Ltd) in PBST. All primary antibodies were incubated overnight at 4°C and secondary antibodies at room temperature for 3h. All washing steps were performed in PBST. Some co-staining required the use of primary antibodies raised in the same species. In these cases, the staining was performed with either pre-conjugated antibodies only, or sequentially using a non-conjugated antibody first, its corresponding secondary antibody next, followed by a blocking step using species-specific serum (3% Goat Serum (G9023-10ML, Sigma) or 3% Rabbit Serum (R9133, Merck)) and finally applying the conjugated antibody. Slide were washed 3 times in PBST and kept sealed at 4°C until imaging.

Primary Antibody	Cat. no, supplier	Dilution
SOX2	14-9811-82, ThermoFisher Scientific	1:200
TBX6	AF4744, R&D Systems	1:400
PAX6	561462, BD Bioscience	1:300
TBXT	NL2085R Conjugated, R&D Systems	1:300
SOX17	AF1924, R&D Systems	1:200
CDX2	Ab76541, Abcam	1:200
OCT4	AP3724A, Abcepta	1:200
FOXA2	8186, Cell Signalling	1:400
SMAD2/3	610842, BD Bioscience	1:100
SOX9	Ab185230 Conjugated, Abcam	1:250
CDH1	SIGMA, MABT26	1:100
CDH2	BD Bioscience, 610182	1:200

Secondary Antibody	Cat. no, supplier	Dilution
Donkey-Anti-Goat-405	Abcam, ab175665	1:1000
Donkey-Anti-Mouse-405	Abcam, ab175658	1:1000
Donkey-Anti-Rat-488	Abcam, ab150153	1:1000
Donkey-Anti-Mouse-488	Abcam, ab150105	1:1000
Donkey-Anti-Rabbit-A568	Abcam, ab175470	1:1000
Donkey-Anti-Mouse-568	Abcam, ab175472	1:1000
Donkey-Anti-Rabbit-647	Abcam, ab150075	1:1000
Donkey-Anti-Rat-647	Abcam, ab150155	1:1000
Donkey-Anti-Mouse-647	Abcam, ab150107	1:1000

Fluorescent In Situ Hybridization

Branched DNA FISH was performed using the viewRNA Cell Plus assay from ThermoFisher Scientific (88-19000-99) according to the manufacturer's protocol. FISH probes used in this study are listed in the table below. Slides were imaged on the same day with a Nikon TiE widefield inverted microscope and a dry 20X lens.

FISH Probe-Channel	Cat.no
NOTO-488	VA4-3101015-VC
CHRD-546	VA1-3005411-VC
NODAL-647	VA6-3167894-VC
LEFTY2-546	VA1-3004742-VC
DKK1-488	VA4-3082344-VC
CER1-488	VA4-3089614-VC

Imaging and Image analysis

Embryos were imaged in PBST using a Leica TCS SP8 Confocal and a 25X water immersion lens. All images were annotated and contrast-adjusted using FIJI (Schindelin et al., 2012). Micropatterned colonies were imaged with an Opera Phenix Plus (Perkin Elmer). Ibidi slides contained around 64 colonies per well, out of which ~20 colonies were selected for analysis in each experiment. To ensure an unbiased sampling of the colonies, the slides were first fully scanned with a 10x lens to generate overview images of the LMBR (nuclear envelope marker) signal only. These images were then processed with an automated pipeline in the harmony software (Perkin Elmer). This pipeline rejected colonies with an unexpected area or roundness and then randomly sampled 20 colonies from the pool of valid colonies. Sampled colonies were next imaged with a 20X lens to generate 3D multichannel z-stacks with voxel size of 0.59 x 0.59 x 1µm. Opera images were then exported as Tiff files for further analysis. Nuclear segmentation was performed on the LMBR signal as described previously (Blin et al., 2019). Raw images and nuclear masks were imported into Pickcells (https://pickcellslab.frama.io/docs/) to compute nuclear features including 3D spatial coordinates and average intensities in all fluorescence channels. The tsv file created in PickCells was then analysed in python. Our Jupyter Notebooks and tsv files are available in our Gitlab repository [Link coming soon].

Nanostring analysis

RNA samples were prepared using an Absolutely RNA microprep kit (cat.no 400805, Agilent technologies) and Nanostring profiling was performed using nCounter technology as per the manufacturer's instructions. We used a panel of probes consisting of the 780 genes included in the standard human embryonic stem cell gene panel together with 30 additional custom probes (listed in Table 1). Normalisation of raw data was accomplished in the Nanostring dedicated nCounter software. Next, raw counts were imported in R (R Core Team, 2013) and analysed with the Bioconductor package moanin (Varoquaux and Purdom, 2020). We first applied an initial cut-off to filter out all the genes where the max count was below 100. The data was then log2 transformed. We kept only the top 50% most variable genes based on the median absolute deviation (mad) metric over time. A spline was then fitted onto each individual gene profile and we grouped genes into 7 clusters using kmeans clustering on the parameters of the fitted splines to obtain the heatmaps shown in Fig 2A. R scripts and data are available in our Gitlab repository [Link coming soon].

Mouse husbandry

Mouse work was carried out under the UK Home Office project license PPL PEEC9E359, approved by the University of Edinburgh Animal Welfare and Ethical Review Panel and in compliance with the Animals (Scientific Procedures) Act 1986. Mice used were of C57Bl6/J strain background. The mice were kept under a 12 h light/dark cycle, and the embryo age was denoted day 0 on the midpoint of the dark cycle the day the plug was found.

Funding:

This work was funded by a BBSRC project grant to GB ref:BB/W002310/1, a BBSRC Alert equipment grant to GB ref: BB/T017961/1 and a WT ISSF3 award to GB ref: IS3-R1.16 19/20. MRG is funded by a BBSRC EASTBIO studentship. EO was funded by a BSDB Gurdon studentship.

Acknowledgements:

We thank Sally Lowell, Anestis Tsakiridis and Val Wilson for their critical review of the manuscript. We also thank Val for helping us with mouse embryos. We thank Justyna Cholewa Waclaw and Matthieu Vermeren or their help with imaging and Alison Munro for running the Nanostring samples.

696 **References**

Abdelkhalek, H. B., Beckers, A., Schuster-Gossler, K., Pavlova, M. N., Burkhardt, H., Lickert, H., Rossant, J., Reinhardt, R., Schalkwyk, L. C., Müller, I., et al. (2004). The mouse homeobox gene Not is required for caudal notochord development and affected by the truncate mutation. *Genes Dev.* **18**, 1725–1736.

Aksoy, I., Giudice, V., Delahaye, E., Wianny, F., Aubry, M., Mure, M., Chen, J., Jauch, R., Bogu, G. K., Nolden, T., et al. (2014). Klf4 and Klf5 differentially inhibit mesoderm and endoderm differentiation in embryonic stem cells. *Nat Commun* **5**, 3719.

Albors, A. R., Halley, P. A. and Storey, K. G. (2018). Lineage tracing of axial progenitors using Nkx1-2CreERT2 mice defines their trunk and tail contributions. *Development* **145**,.

Ang, S. L. and Rossant, J. (1994). HNF-3 beta is essential for node and notochord formation in mouse development. *Cell* **78**, 561–574.

Arnold, S. J., Stappert, J., Bauer, A., Kispert, A., Herrmann, B. G. and Kemler, R. (2000). Brachyury is a target gene of the Wnt/beta-catenin signaling pathway. *Mech. Dev.* **91**, 249–258.

Avilion, A. A., Nicolis, S. K., Pevny, L. H., Perez, L., Vivian, N. and Lovell-Badge, R. (2003). Multipotent cell lineages in early mouse development depend on SOX2 function. *Genes Dev* **17**, 126–140.

Bachiller, D., Klingensmith, J., Kemp, C., Belo, J. A., Anderson, R. M., May, S. R., McMahon, J. A., McMahon, A. P., Harland, R. M., Rossant, J., et al. (2000). The organizer factors Chordin and Noggin are required for mouse forebrain development. *Nature* **403**, 658–661.

Bagheri-Fam, S., Barrionuevo, F., Dohrmann, U., Günther, T., Schüle, R., Kemler, R., Mallo, M., Kanzler, B. and Scherer, G. (2006). Long-range upstream and downstream enhancers control distinct subsets of the complex spatiotemporal Sox9 expression pattern. *Developmental Biology* **291**, 382–397.

Bagnat, M. and Gray, R. S. (2020). Development of a straight vertebrate body axis. *Development* **147**,.

Bakker, B. S. de, Jong, K. H. de, Hagoort, J., Bree, K. de, Besselink, C. T., Kanter, F. E. C. de, Veldhuis, T., Bais, B., Schildmeijer, R., Ruijter, J. M., et al. (2016). An interactive three-dimensional digital atlas and quantitative database of human development. *Science* **354**, aag0053.

Balmer, S., Nowotschin, S. and Hadjantonakis, A.-K. (2016). Notochord morphogenesis in mice: Current understanding & open questions. *Developmental Dynamics* **245**, 547–557.

Bardot, E., Calderon, D., Santoriello, F., Han, S., Cheung, K., Jadhav, B., Burtscher, I., Artap, S., Jain, R., Epstein, J., et al. (2017). Foxa2 identifies a cardiac progenitor population with ventricular differentiation potential. *Nat Commun* **8**, 14428.

Beccari, L., Moris, N., Girgin, M., Turner, D. A., Baillie-Johnson, P., Cossy, A.-C., Lutolf, M. P., Duboule, D. and Arias, A. M. (2018). Multi-axial self-organization properties of mouse embryonic stem cells into gastruloids. *Nature* **562**, 272–276.

Beddington, R. S. and Robertson, E. J. (1989). An assessment of the developmental potential of embryonic stem cells in the midgestation mouse embryo. *Development* **105**, 733–737.

Belo, J. A., Bouwmeester, T., Leyns, L., Kertesz, N., Gallo, M., Follettie, M. and De Robertis, E. M. (1997). Cerberus-like is a secreted factor with neutralizing activity expressed in the anterior primitive endoderm of the mouse gastrula. *Mech. Dev.* **68**, 45–57.

Ben-Haim, N., Lu, C., Guzman-Ayala, M., Pescatore, L., Mesnard, D., Bischofberger, M., Naef, F., Robertson, E. J. and Constam, D. B. (2006). The nodal precursor acting via activin receptors induces mesoderm by maintaining a source of its convertases and BMP4. *Dev. Cell* **11**, 313–323.

Blin, G. (2021). Quantitative developmental biology in vitro using micropatterning. *Development* **148**,.

Blin, G., Sadurska, D., Migueles, R. P., Chen, N., Watson, J. A. and Lowell, S. (2019). Nessys: A new set of tools for the automated detection of nuclei within intact tissues and dense 3D cultures. *PLOS Biology* **17**, e3000388.

Burtscher, I. and Lickert, H. (2009). Foxa2 regulates polarity and epithelialization in the endoderm germ layer of the mouse embryo. *Development* **136**, 1029–1038.

C, M., G, C., Ka, J., Ac, H., Gg, S. and J, N. (2018). Oct4 regulates the embryonic axis and coordinates exit from pluripotency and germ layer specification in the mouse embryo. *Development (Cambridge, England)* **145**,.

Cadigan, K. M. and Waterman, M. L. (2012). TCF/LEFs and Wnt Signaling in the Nucleus. *Cold Spring Harb Perspect Biol* **4**, a007906.

Cambray, N. and Wilson, V. (2002). Axial progenitors with extensive potency are localised to the mouse chordoneural hinge. *Development* **129**, 4855–4866.

Cambray, N. and Wilson, V. (2007). Two distinct sources for a population of maturing axial progenitors. *Development* **134**, 2829–2840.

Cermola, F., D'Aniello, C., Tatè, R., Cesare, D. D., Martinez-Arias, A., Minchiotti, G. and Patriarca, E. J. (2021). Gastruloid Development Competence Discriminates Different States of Pluripotency. *Stem Cell Reports* **16**, 354–369.

Chen, B., Dodge, M. E., Tang, W., Lu, J., Ma, Z., Fan, C.-W., Wei, S., Hao, W., Kilgore, J., Williams, N. S., et al. (2009). Small molecule-mediated disruption of Wnt-dependent signaling in tissue regeneration and cancer. *Nat Chem Biol* **5**, 100–107.

Chhabra, S., Liu, L., Goh, R., Kong, X. and Warmflash, A. (2019). Dissecting the dynamics of signaling events in the BMP, WNT, and NODAL cascade during self-organized fate patterning in human gastruloids. *PLOS Biology* **17**, e3000498.

Choi, K.-S., Cohn, M. J. and Harfe, B. D. (2008). Identification of nucleus pulposus precursor cells and notochordal remnants in the mouse: Implications for disk degeneration and chordoma formation. *Developmental Dynamics* **237**, 3953–3958.

Colombier, P., Halgand, B., Chédeville, C., Chariau, C., François-Campion, V., Kilens, S., Vedrenne, N., Clouet, J., David, L., Guicheux, J., et al. (2020). NOTO Transcription Factor Directs Human Induced Pluripotent Stem Cell-Derived Mesendoderm Progenitors to a Notochordal Fate. *Cells* **9**, 509.

Costello, I., Pimeisl, I.-M., Dräger, S., Bikoff, E. K., Robertson, E. J. and Arnold, S. J. (2011). The T-box transcription factor Eomesodermin acts upstream of Mesp1 to specify cardiac mesoderm during mouse gastrulation. *Nat Cell Biol* **13**, 1084–1091.

Costello, I., Nowotschin, S., Sun, X., Mould, A. W., Hadjantonakis, A.-K., Bikoff, E. K. and Robertson, E. J. (2015). Lhx1 functions together with Otx2, Foxa2, and Ldb1 to govern anterior mesendoderm, node, and midline development. *Genes Dev* **29**, 2108–2122.

Diaz-Hernandez, M. E., Khan, N. M., Trochez, C. M., Yoon, T., Maye, P., Presciutti, S. M., Gibson, G. and Drissi, H. (2020). Derivation of notochordal cells from human embryonic stem cells reveals unique regulatory networks by single cell-transcriptomics. *Journal of Cellular Physiology* **235**, 5241–5255.

Dunn, N. R., Vincent, S. D., Oxburgh, L., Robertson, E. J. and Bikoff, E. K. (2004). Combinatorial activities of Smad2 and Smad3 regulate mesoderm formation and patterning in the mouse embryo. *Development* **131**, 1717–1728.

Edri, S., Hayward, P., Jawaid, W. and Arias, A. M. (2019). Neuro-mesodermal progenitors (NMPs): a comparative study between pluripotent stem cells and embryo-derived populations. *Development* **146**, dev180190.

Etoc, F., Metzger, J., Ruzo, A., Kirst, C., Yoney, A., Ozair, M. Z., Brivanlou, A. H. and Siggia, E. D. (2016). A Balance between Secreted Inhibitors and Edge Sensing Controls Gastruloid Self-Organization. *Developmental Cell* **39**, 302–315.

Fang, P.-K., Solomon, K. R., Zhuang, L., Qi, M., McKee, M., Freeman, M. R. and Yelick, P. C. (2006). Caveolin-1α and −1β Perform Nonredundant Roles in Early Vertebrate Development. *The American Journal of Pathology* **169**, 2209–2222.

Forlani, S., Lawson, K. A. and Deschamps, J. (2003). Acquisition of Hox codes during gastrulation and axial elongation in the mouse embryo. *Development* **130**, 3807–3819.

Frith, T. J. R. and Tsakiridis, A. (2019). Efficient Generation of Trunk Neural Crest and Sympathetic Neurons from Human Pluripotent Stem Cells Via a Neuromesodermal Axial Progenitor Intermediate. *Current Protocols in Stem Cell Biology* **49**, e81.

Frith, T. J., Granata, I., Wind, M., Stout, E., Thompson, O., Neumann, K., Stavish, D., Heath, P. R., Ortmann, D., Hackland, J. O., et al. (2018). Human axial progenitors generate trunk neural crest cells in vitro. *eLife* **7**, e35786.

Gouti, M., Tsakiridis, A., Wymeersch, F. J., Huang, Y., Kleinjung, J., Wilson, V. and Briscoe, J. (2014). In Vitro Generation of Neuromesodermal Progenitors Reveals Distinct Roles for Wnt Signalling in the Specification of Spinal Cord and Paraxial Mesoderm Identity. *PLOS Biology* **12**, e1001937.

Hart, A. H., Hartley, L., Sourris, K., Stadler, E. S., Li, R., Stanley, E. G., Tam, P. P. L., Elefanty, A. G. and Robb, L. (2002). Mixl1 is required for axial mesendoderm morphogenesis and patterning in the murine embryo. *Development* **129**, 3597–3608.

Hart, A. H., Hartley, L., Ibrahim, M. and Robb, L. (2004). Identification, cloning and expression analysis of the pluripotency promoting Nanog genes in mouse and human. *Developmental Dynamics* **230**, 187–198.

Heemskerk, I. (2019). Full of potential: Pluripotent stem cells for the systems biology of embryonic patterning. *Developmental Biology*.

Henrique, D., Abranches, E., Verrier, L. and Storey, K. G. (2015). Neuromesodermal progenitors and the making of the spinal cord. *Development* **142**, 2864–2875.

Inman, G. J., Nicolás, F. J., Callahan, J. F., Harling, J. D., Gaster, L. M., Reith, A. D., Laping, N. J. and Hill, C. S. (2002). SB-431542 is a potent and specific inhibitor of transforming growth factor-beta superfamily type I activin receptor-like kinase (ALK) receptors ALK4, ALK5, and ALK7. *Mol Pharmacol* **62**, 65–74.

Kanai-Azuma, M., Kanai, Y., Gad, J. M., Tajima, Y., Taya, C., Kurohmaru, M., Sanai, Y., Yonekawa, H., Yazaki, K., Tam, P. P. L., et al. (2002). Depletion of definitive gut endoderm in Sox17-null mutant mice. *Development* **129**, 2367–2379.

Kinder, S. J., Tsang, T. E., Wakamiya, M., Sasaki, H., Behringer, R. R., Nagy, A. and Tam, P. P. L. (2001). The organizer of the mouse gastrula is composed of a dynamic population of progenitor cells for the axial mesoderm. *Development* **128**, 3623–3634.

Koch, F., Scholze, M., Wittler, L., Schifferl, D., Sudheer, S., Grote, P., Timmermann, B., Macura, K. and Herrmann, B. G. (2017). Antagonistic Activities of Sox2 and Brachyury Control the Fate Choice of Neuro-Mesodermal Progenitors. *Developmental Cell* **42**, 514-526.e7.

Kwon, G. S., Viotti, M. and Hadjantonakis, A.-K. (2008). The Endoderm of the Mouse Embryo Arises by Dynamic Widespread Intercalation of Embryonic and Extraembryonic Lineages. *Developmental Cell* **15**, 509–520.

Lawson, K. A., Meneses, J. J. and Pedersen, R. A. (1991). Clonal analysis of epiblast fate during germ layer formation in the mouse embryo. *Development* **113**, 891–911.

Legier, T., Rattier, D., Llewellyn, J., Vannier, T., Sorre, B., Maina, F. and Dono, R. (2023). Epithelial disruption drives mesendoderm differentiation in human pluripotent stem cells by enabling TGF-β protein sensing. *Nat Commun* **14**, 349.

Lickert, H., Kutsch, S., Kanzler, B., Tamai, Y., Taketo, M. M. and Kemler, R. (2002). Formation of multiple hearts in mice following deletion of beta-catenin in the embryonic endoderm. *Dev Cell* **3**, 171–181.

Lolas, M., Valenzuela, P. D. T., Tjian, R. and Liu, Z. (2014). Charting Brachyury-mediated developmental pathways during early mouse embryogenesis. *PNAS* **111**, 4478–4483.

Martins, J.-M. F., Fischer, C., Urzi, A., Vidal, R., Kunz, S., Ruffault, P.-L., Kabuss, L., Hube, I., Gazzerro, E., Birchmeier, C., et al. (2020). Self-Organizing 3D Human Trunk Neuromuscular Organoids. *Cell Stem Cell* **26**, 172-186.e6.

Martyn, I., Kanno, T. Y., Ruzo, A., Siggia, E. D. and Brivanlou, A. H. (2018). Self-organization of a human organizer by combined Wnt and Nodal signalling. *Nature* **558**, 132–135.

Martyn, I., Brivanlou, A. H. and Siggia, E. D. (2019). A wave of WNT signaling balanced by secreted inhibitors controls primitive streak formation in micropattern colonies of human embryonic stem cells. *Development* **146**,.

Massey, J., Liu, Y., Alvarenga, O., Saez, T., Schmerer, M. and Warmflash, A. (2019). Synergy with TGFβ ligands switches WNT pathway dynamics from transient to sustained during human pluripotent cell differentiation. *PNAS* **116**, 4989–4998.

McCann, M. R., Tamplin, O. J., Rossant, J. and Séguin, C. A. (2012). Tracing notochord-derived cells using a Noto-cre mouse: implications for intervertebral disc development. *Dis Model Mech* **5**, 73–82.

Merrill, B. J., Pasolli, H. A., Polak, L., Rendl, M., García-García, M. J., Anderson, K. V. and Fuchs, E. (2004). Tcf3: a transcriptional regulator of axis induction in the early embryo. *Development* **131**, 263–274.

Moore-Scott, B. A., Opoka, R., Lin, S.-C. J., Kordich, J. J. and Wells, J. M. (2007). Identification of molecular markers that are expressed in discrete anterior–posterior domains of the endoderm from the gastrula stage to mid-gestation. *Developmental Dynamics* **236**, 1997–2003.

Moris, N., Anlas, K., van den Brink, S. C., Alemany, A., Schröder, J., Ghimire, S., Balayo, T., van Oudenaarden, A. and Martinez Arias, A. (2020). An in vitro model of early anteroposterior organization during human development. *Nature* **582**, 410–415.

Morrisey, E. E., Ip, H. S., Lu, M. M. and Parmacek, M. S. (1996). GATA-6: a zinc finger transcription factor that is expressed in multiple cell lineages derived from lateral mesoderm. *Dev Biol* **177**, 309–322.

Neijts, R., Simmini, S., Giuliani, F., van Rooijen, C. and Deschamps, J. (2014). Region-specific regulation of posterior axial elongation during vertebrate embryogenesis. *Developmental Dynamics* **243**, 88–98.

Norris, D. P., Brennan, J., Bikoff, E. K. and Robertson, E. J. (2002). The Foxh1-dependent autoregulatory enhancer controls the level of Nodal signals in the mouse embryo. *Development* **129**, 3455–3468.

Olmsted, Z. T. and Paluh, J. L. (2021). Co-development of central and peripheral neurons with trunk mesendoderm in human elongating multi-lineage organized gastruloids. *Nat Commun* **12**, 3020.

Osorno, R., Tsakiridis, A., Wong, F., Cambray, N., Economou, C., Wilkie, R., Blin, G., Scotting, P. J., Chambers, I. and Wilson, V. (2012). The developmental dismantling of pluripotency is reversed by ectopic Oct4 expression. *Development* **139**, 2288–2298.

Perea-Gomez, A., Vella, F. D. J., Shawlot, W., Oulad-Abdelghani, M., Chazaud, C., Meno, C., Pfister, V., Chen, L., Robertson, E., Hamada, H., et al. (2002). Nodal antagonists in the anterior visceral endoderm prevent the formation of multiple primitive streaks. *Dev. Cell* **3**, 745–756.

Plouhinec, J.-L., Granier, C., Le Mentec, C., Lawson, K. A., Sabéran-Djoneidi, D., Aghion, J., Shi, D. L., Collignon, J. and Mazan, S. (2004). Identification of the mammalian Not gene via a phylogenomic approach. *Gene Expression Patterns* **5**, 11–22.

Plouhinec, J.-L., Simon, G., Vieira, M., Collignon, J. and Sorre, B. (2022). Dissecting signaling hierarchies in the patterning of the mouse primitive streak using micropatterned EpiLC colonies. *Stem Cell Reports* **17**, 1757–1771.

Pour, M., Kumar, A. S., Farag, N., Bolondi, A., Kretzmer, H., Walther, M., Wittler, L., Meissner, A. and Nachman, I. (2022). Emergence and patterning dynamics of mouse-definitive endoderm. *iScience* **25**, 103556.

R Core Team (2013). *R: A Language and Environment for Statistical Computing*. Vienna, Austria: R Foundation for Statistical Computing.

Rito, T., Libby, A. R. G., Demuth, M. and Briscoe, J. (2023). Notochord and axial progenitor generation by timely BMP and NODAL inhibition during vertebrate trunk formation. 2023.02.27.530267.

Robertson, E. J. (2014). Dose-dependent Nodal/Smad signals pattern the early mouse embryo. *Seminars in Cell & Developmental Biology* **32**, 73–79.

Sanaki-Matsumiya, M., Matsuda, M., Gritti, N., Nakaki, F., Sharpe, J., Trivedi, V. and Ebisuya, M. (2022). Periodic formation of epithelial somites from human pluripotent stem cells. *Nat Commun* **13**, 2325.

Scheibner, K., Schirge, S., Burtscher, I., Büttner, M., Sterr, M., Yang, D., Böttcher, A., Ansarullah, Irmler, M., Beckers, J., et al. (2021). Epithelial cell plasticity drives endoderm formation during gastrulation. *Nat Cell Biol* **23**, 692–703.

Schindelin, J., Arganda-Carreras, I., Frise, E., Kaynig, V., Longair, M., Pietzsch, T., Preibisch, S., Rueden, C., Saalfeld, S., Schmid, B., et al. (2012). Fiji: an open-source platform for biological-image analysis. *Nature Methods* **9**, 676–682.

Schohl, A. and Fagotto, F. (2002). Beta-catenin, MAPK and Smad signaling during early Xenopus development. *Development* **129**, 37–52.

Semënov, M. V., Tamai, K., Brott, B. K., Kühl, M., Sokol, S. and He, X. (2001). Head inducer Dickkopf-1 is a ligand for Wnt coreceptor LRP6. *Curr Biol* **11**, 951–961.

Stemple, D. L. (2005). Structure and function of the notochord: an essential organ for chordate development. *Development* **132**, 2503–2512.

Streit, A. and Stern, C. D. (1999). Mesoderm patterning and somite formation during node regression: differential effects of chordin and noggin. *Mech Dev* **85**, 85–96.

Sulik, K., Dehart, D. B., Inagaki, T., Carson, J. L., Vrablic, T., Gesteland, K. and Schoenwolf, G. C. (1994). Morphogenesis of the murine node and notochordal plate. *Developmental Dynamics* **201**, 260–278.

Tam, P. P., Parameswaran, M., Kinder, S. J. and Weinberger, R. P. (1997). The allocation of epiblast cells to the embryonic heart and other mesodermal lineages: the role of ingression and tissue movement during gastrulation. *Development* **124**, 1631–1642.

Tamplin, O. J., Cox, B. J. and Rossant, J. (2011). Integrated microarray and ChIP analysis identifies multiple Foxa2 dependent target genes in the notochord. *Dev Biol* **360**, 415–425.

Tsakiridis, A., Huang, Y., Blin, G., Skylaki, S., Wymeersch, F., Osorno, R., Economou, C., Karagianni, E., Zhao, S., Lowell, S., et al. (2014). Distinct Wnt-driven primitive streak-like populations reflect in vivo lineage precursors. *Development* **141**, 1209–1221.

Turner, D. A., Hayward, P. C., Baillie-Johnson, P., Rué, P., Broome, R., Faunes, F. and Arias, A. M. (2014). Wnt/β-catenin and FGF signalling direct the specification and maintenance of a neuromesodermal axial progenitor in ensembles of mouse embryonic stem cells. *Development* **141**, 4243–4253.

Turner, D. A., Girgin, M., Alonso-Crisostomo, L., Trivedi, V., Baillie-Johnson, P., Glodowski, C. R., Hayward, P. C., Collignon, J., Gustavsen, C., Serup, P., et al. (2017). Anteroposterior polarity and elongation in the absence of extra-embryonic tissues and of spatially localised signalling in gastruloids: mammalian embryonic organoids. *Development* **144**, 3894–3906.

Tzouanacou, E., Wegener, A., Wymeersch, F. J., Wilson, V. and Nicolas, J.-F. (2009). Redefining the Progression of Lineage Segregations during Mammalian Embryogenesis by Clonal Analysis. *Developmental Cell* **17**, 365–376.

Ukita, K., Hirahara, S., Oshima, N., Imuta, Y., Yoshimoto, A., Jang, C.-W., Oginuma, M., Saga, Y., Behringer, R. R., Kondoh, H., et al. (2009). Wnt signaling maintains the notochord fate for progenitor cells and supports the posterior extension of the notochord. *Mechanisms of Development* **126**, 791–803.

Varoquaux, N. and Purdom, E. (2020). A pipeline to analyse time-course gene expression data.

Veenvliet, J. V., Bolondi, A., Kretzmer, H., Haut, L., Scholze-Wittler, M., Schifferl, D., Koch, F., Guignard, L., Kumar, A. S., Pustet, M., et al. (2020). Mouse embryonic stem cells self-organize into trunk-like structures with neural tube and somites. *Science* **370**, eaba4937.

Vincent, S. D., Dunn, N. R., Hayashi, S., Norris, D. P. and Robertson, E. J. (2003). Cell fate decisions within the mouse organizer are governed by graded Nodal signals. *Genes Dev.* **17**, 1646–1662.

Viotti, M., Nowotschin, S. and Hadjantonakis, A.-K. (2014). SOX17 links gut endoderm morphogenesis and germ layer segregation. *Nature Cell Biology* **16**, 1146–1156.

Warmflash, A., Sorre, B., Etoc, F., Siggia, E. D. and Brivanlou, A. H. (2014). A method to recapitulate early embryonic spatial patterning in human embryonic stem cells. *Nat Meth* **11**, 847–854.

Washkowitz, A. J., Gavrilov, S., Begum, S. and Papaioannou, V. E. (2012). Diverse functional networks of Tbx3 in development and disease. *Wiley Interdiscip Rev Syst Biol Med* **4**, 273–283.

Winzi, M. K., Hyttel, P., Dale, J. K. and Serup, P. (2011). Isolation and characterization of node/notochord-like cells from mouse embryonic stem cells. *Stem Cells and Development* **20**, 1817–1828.

Wise, C. A., Sepich, D., Ushiki, A., Khanshour, A. M., Kidane, Y. H., Makki, N., Gurnett, C. A., Gray, R. S., Rios, J. J., Ahituv, N., et al. (2020). The cartilage matrisome in adolescent idiopathic scoliosis. *Bone Research* **8**, 1–13.

Wisniewski, D., Lowell, S. and Blin, G. (2019). Mapping the Emergent Spatial Organization of Mammalian Cells using Micropatterns and Quantitative Imaging. *J Vis Exp*.

Wymeersch, F. J., Skylaki, S., Huang, Y., Watson, J. A., Economou, C., Marek-Johnston, C., Tomlinson, S. R. and Wilson, V. (2019). Transcriptionally dynamic progenitor populations organised around a stable niche drive axial patterning. *Development* **146**,.

Wymeersch, F. J., Wilson, V. and Tsakiridis, A. (2021). Understanding axial progenitor biology in vivo and in vitro. *Development* **148**,.

Xu, P.-F., Borges, R. M., Fillatre, J., de Oliveira-Melo, M., Cheng, T., Thisse, B. and Thisse, C. (2021). Construction of a mammalian embryo model from stem cells organized by a morphogen signalling centre. *Nat Commun* **12**, 3277.

Yamamoto, M., Meno, C., Sakai, Y., Shiratori, H., Mochida, K., Ikawa, Y., Saijoh, Y. and Hamada, H. (2001). The transcription factor FoxH1 (FAST) mediates Nodal signaling during anterior-posterior patterning and node formation in the mouse. *Genes Dev* **15**, 1242–1256.

Yamanaka, Y., Tamplin, O. J., Beckers, A., Gossler, A. and Rossant, J. (2007). Live Imaging and Genetic Analysis of Mouse Notochord Formation Reveals Regional Morphogenetic Mechanisms. *Developmental Cell* **13**, 884–896.

Yasuo, H. and Lemaire, P. (2001). Role of Goosecoid, Xnot and Wnt antagonists in the maintenance of the notochord genetic programme in Xenopus gastrulae. *Development* **128**, 3783–3793.

Yoney, A., Etoc, F., Ruzo, A., Carroll, T., Metzger, J. J., Martyn, I., Li, S., Kirst, C., Siggia, E. D. and Brivanlou, A. H. (2018). WNT signaling memory is required for ACTIVIN to function as a morphogen in human gastruloids. *eLife* **7**, e38279.

Yoney, A., Bai, L., Brivanlou, A. H. and Siggia, E. D. (2022). Mechanisms underlying WNT-mediated priming of human embryonic stem cells. *Development* **149**, dev200335.

Zhang, Y., Zhang, Z., Chen, P., Ma, C. Y., Li, C., Au, T. Y. K., Tam, V., Peng, Y., Wu, R., Cheung, K. M. C., et al. (2020). Directed Differentiation of Notochord-like and Nucleus Pulposus-like Cells Using Human Pluripotent Stem Cells. *Cell Reports* **30**, 2791-2806.e5.

Zhao, R., Watt, A. J., Li, J., Luebke-Wheeler, J., Morrisey, E. E. and Duncan, S. A. (2005). GATA6 Is Essential for Embryonic Development of the Liver but Dispensable for Early Heart Formation. *Mol Cell Biol* **25**, 2622–2631.

697